TECHNICAL ARTICLE

Order and disorder in NMC layered materials: a FAULTS simulation analysis

Marine Reynaud and Montse Casas-Cabanas[a)]
CIC Energigune, Parque Tecnológico de Álava, Albert Einstein 48, 01510 Miñano, Spain

(Received 16 October 2016; accepted 1 January 2017)

The program FAULTS has been used to simulate the X-ray powder diffraction (XRD), neutron powder diffraction (NPD), and electron diffraction (ED) patterns of several structural models for $LiNi_{1/3}Mn_{1/3}Co_{1/3}O_2$, including different types of ordering of the transition metal (TM) cations in the TM slabs, different amounts of Li^{+}/Ni^{II+} cation mixing and different amounts of stacking faults. The results demonstrate the relevance of the structural information provided by NPD and ED data as compared with XRD to characterize the microstructure of NMC ($LiNi_{1-y-z}Mn_yCo_zO_2$) compounds. © *2017 International Centre for Diffraction Data*. [doi:10.1017/S0885715617000033]

Key words: X-ray powder diffraction, neutron powder diffraction, electron diffraction, diffuse scattering, stacking faults, layered materials, FAULTS, DIFFaX, battery materials, layered oxide

I. INTRODUCTION

The first commercialization of Li-ion batteries by SONY in 1991 was made possible thanks to the innovative selection of a graphite negative electrode and a lithium cobalt oxide as the positive electrode (Nagaura and Tozawa, 1990; Tarascon and Armand, 2001; Rozier and Tarascon, 2015). This $LiCoO_2$/C technology is still used in a great part of current Li-ion batteries, although other lithium metal oxides (derivatives of $LiCoO_2$), spinel-like compounds ($LiMn_2O_4$), or polyanionic compounds ($LiFePO_4$) are steadily gaining market share. Indeed the energy load of $LiCoO_2$/C cells cannot be fully exploited but must be limited to half (~140 mAh g^{-1} of $LiCoO_2$) of their theoretical capacity (275 mAh g^{-1} of $LiCoO_2$) to avoid positive electrode degradation and potential associated hazards. The last two decades have witnessed a huge amount of research on the partial substitution of Co^{III+} by Al^{III+}, Ni^{II+}, Mn^{IV+} to enhance the performance of the cathode material in terms of capacity, rate capability and structural stability, which led to the attractive compounds $LiNi_{1-y-z}Co_yAl_zO_2$ and $LiNi_{1-y-z}Mn_yCo_zO_2$ (NMC) (Lu *et al.*, 2001; Madhavi *et al.*, 2001; Ohzuku and Makimura, 2001; Weaving *et al.*, 2001; Guilmard *et al.*, 2003; Hwang *et al.*, 2003; Yabuuchi and Ohzuku, 2003). Among all the compositions studied, $LiNi_{1/3}Mn_{1/3}Co_{1/3}O_2$ has shown particularly promising electrochemical performances with reversible capacity reaching up to 200 mAh g^{-1} together with enhanced thermal stability, and it is now widely used as cathode material for numerous commercial applications (Yin *et al.*, 2006; Rozier and Tarascon, 2015).

Layered oxides $LiMO_2$ (M = Co, Ni, Mn) adopt the α-$NaFeO_2$ structure, which corresponds to an ordered rock salt in which lithium cations and transition metal (TM) cations alternatively occupy the successive layers of octahedral sites of the face-centered cubic array of oxygen anions, leading to a regular stacking of LiO_2 and MO_2 sheets along the $[111]_{FCC}$ direction (Figure 1). Delmas *et al.* proposed a classification of the different possibilities of stacking that can be obtained, indicating the coordination of the alkali cation in the interslabs (T for tetrahedral, O for octahedral, and P for prismatic) and the number of MO_2 slabs needed to recover the periodicity (Delmas *et al.*, 1980).

The average structure of NMC compounds is usually described as an O3-type stacking with a trigonal R-3m unit cell (hexagonal setting) or with a monoclinic $C$2/m unit cell (Figure 1). However, there are still discrepancies about the real structure of these compounds. Depending on the preparation history of the samples, the techniques used for their characterization and the interpretation of the results, the following features have been reported by different groups having studied

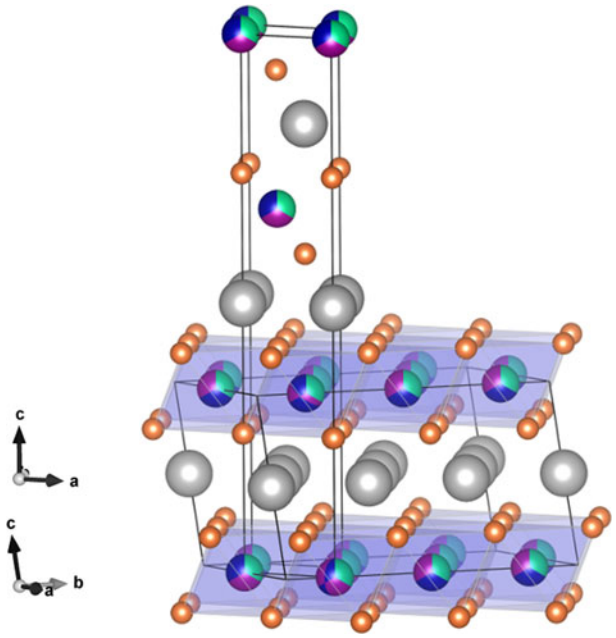

Figure 1. (Colour online) Ideal structure of $LiNi_{1/3}Mn_{1/3}Co_{1/3}O_2$ described in both the R-3m trigonal and the $C$2/m monoclinic cells. MO_6 octahedra are drawn in blue, where M = Ni, Co, Mn are shown as green, blue, and purple balls, respectively. Lithium cations and oxygen anions are pictured as gray, and orange balls, respectively.

[a)]Author to whom correspondence should be addressed. Electronic mail: mcasas@cicenergigune.com

TABLE I. Structural model used in FAULTS for the simulation of the XRD, NPD, and SADP patterns of $LiNi_{1/3}Mn_{1/3}Co_{1/3}O_2$, in the case of *fully ordered* TM cation slabs, without Li^+/Ni^{II+} cation mixing and with stacking faults occurring with a probability $p = 10$ %.

Cell					
$a = 4.95$ Å		$b = 8.58$ Å	$c' = 4.739\,906$ Å		
$\alpha = 90°$		$\beta = 90°$	$\gamma = 90°$		
Layers					
	Atom (#)	*x/a*	*y/b*	*z/c*	B_{iso}
Layer 1	Ni^{II+} (1)	0	1/6	0	0.5
=Layer 3	Mn^{IV+} (2)	0	5/6	0	0.5
=Layer 4	Ni^{II+} (3)	1/2	2/3	0	0.5
	Mn^{IV+} (4)	1/2	1/3	0	0.5
	Co^{III+} (5)	0	1/2	0	0.5
	Co^{III+} (6)	1/2	0	0	0.5
Layer 2	Li^+ (7)	0	0	0	0.5
	Li^+ (8)	1/2	1/2	0	0.5
	Li^+ (9)	0	2/3	0	0.5
	Li^+ (10)	0	1/3	0	0.5
	Li^+ (11)	1/2	1/6	0	0.5
	Li^+ (12)	1/2	5/6	0	0.5
	O^{II-} (13)	0.341 666 7	0	−0.275	0.5
	O^{II-} (14)	0.658 333 3	0	0.275	0.5
	O^{II-} (15)	0.841 666 7	1/2	−0.275	0.5
	O^{II-} (16)	0.158 333 3	1/2	0.275	0.5
	O^{II-} (17)	0.341 666 7	1/3	−0.275	0.5
	O^{II-} (18)	0.658 333 3	2/3	0.275	0.5
	O^{II-} (19)	0.658 333 3	1/3	0.275	0.5
	O^{II-} (20)	0.341 666 7	2/3	−0.275	0.5
	O^{II-} (21)	0.841 666 7	5/6	−0.275	0.5
	O^{II-} (22)	0.158 333 3	1/6	0.275	0.5
	O^{II-} (23)	0.158 333 3	5/6	0.275	0.5
	O^{II-} (24)	0.841 666 7	1/6	−0.275	0.5
Stacking transition vectors					
Transition		*x/a*	*y/b*	*z/c´*	*p*
Layer 1 → Layer 1		–	–	–	0.0
→ Layer 2		−1/6	0	1/2	1.0
→ Layer 3		–	–	–	0.0
→ Layer 4		–	–	–	0.0
Layer 2 → Layer 1		−1/6	0	1/2	0.9
→ Layer 2		–	–	–	0.0
→ Layer 3		−1/6	1/3	1/2	0.1
→ Layer 4		−1/6	−1/3	1/2	0.1
Layer 3 → Layer 1		–	–	–	0.0
→ Layer 2		−1/6	0	1/2	1.0
→ Layer 3		–	–	–	0.0
→ Layer 4		–	–	–	0.0
Layer 4 → Layer 1		–	–	–	0.0
→ Layer 2		−1/6	0	1/2	1.0
→ Layer 3		–	–	–	0.0
→ Layer 4		–	–	–	0.0

these compounds: (i) random distribution of the cations within the TM slabs (Kim and Chung, 2004; Whitfield *et al.*, 2005); (ii) existence of local ordering (Cahill *et al.*, 2005; Tsai *et al.*, 2005; Zeng *et al.*, 2007; Shinova *et al.*, 2008); or (iii) long-range ordering of the cations leading to a superstructure (Koyama *et al.*, 2003); (iv) presence of stacking faults (Yabuuchi *et al.*, 2005); and (v) Li^+/Ni^{II+} cation mixing between the Li and Ni sites between the TM slabs and Li inter-slabs (from 0 to 10% depending of the reports) (Kim and Chung, 2004; Cahill *et al.*, 2005; Whitfield *et al.*, 2005; Yin *et al.*, 2006). Indeed such controversies are probably because of the fact that the microstructure of the sample may vary depending on their preparation condition, but also owing to a lack of thorough characterization studies combining several

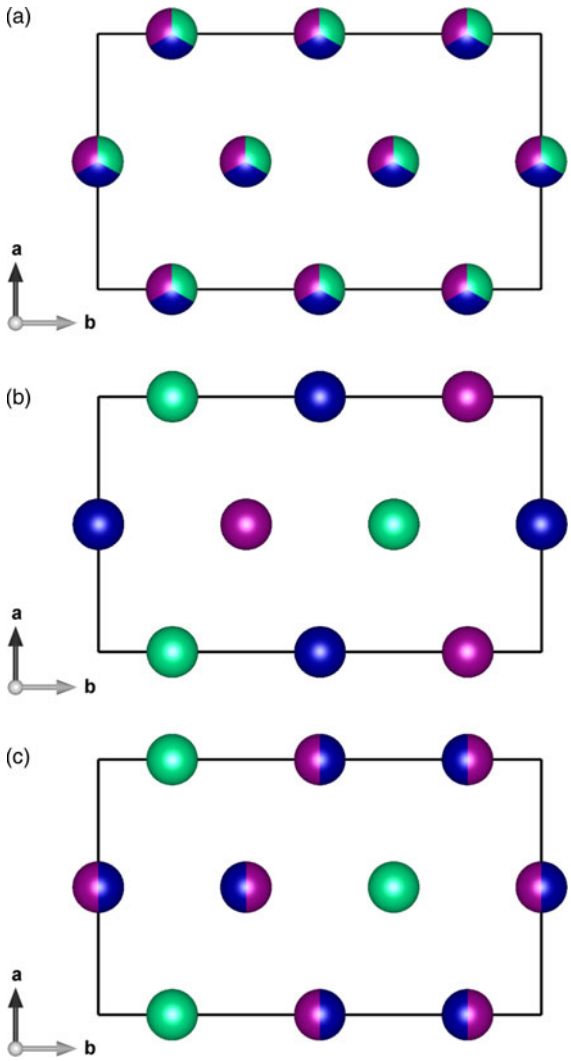

Figure 2. (Colour online) Different models explored for the TM cation distribution within the TM layers (layer 1): (a) *random* model, (b) *fully ordered* model, and (c) *honeycomb* models. Ni^{II+}, Mn^{IV+} and Co^{III+} cations are drawn as spheres colored in green, purple and blue, respectively.

complementary techniques [both at a long-range scale: X-ray powder diffraction (XRD), neutron powder diffraction (NPD), and a more local one: electron diffraction (ED), NMR, etc.] and difficulties in the analysis and interpretation of the results.

Here we used the program FAULTS to simulate the XRD, NPD, and ED patterns of different structural models for $LiNi_{1/3}Mn_{1/3}Co_{1/3}O_2$ compounds (Casas-Cabanas *et al.*, 2006, 2015, 2016). We demonstrate the importance of combining different techniques to carefully characterize NMC samples, and we show the advantages of using the program FAULTS for the refinement of the powder diffraction patterns instead of conventional Rietveld methods.

II. METHOD

The program FAULTS can perform the simulation of X-ray, neutron, and electron diffraction patterns of defective layered materials, as well as the refinement of their X-ray and neutron powder patterns (Casas-Cabanas *et al.*, 2006, 2015, 2016). FAULTS is a FORTRAN 90 program, based on the kernel of the DIFFaX program (Treacy *et al.*, 1991a,

https://doi.org/10.1017/S0885715617000033 Published online by Cambridge University Press

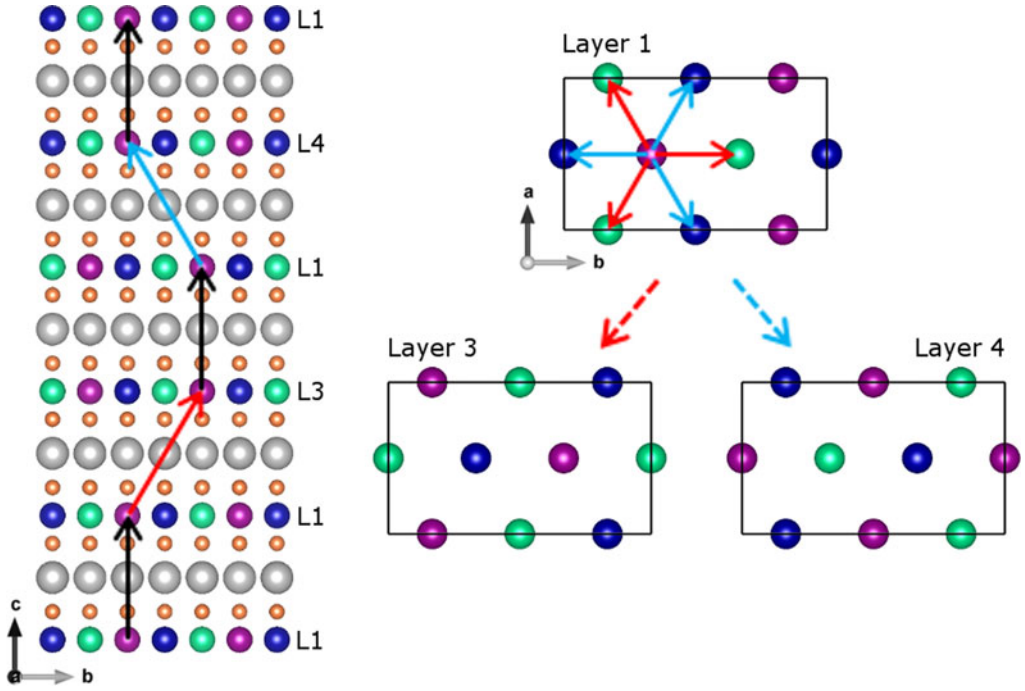

Figure 3. (Colour online) Introduction of stacking faults in the stacking of the layers by means of the different transition vectors ($t_{L1\rightarrow L1}$ as a black arrow, $t_{L1\rightarrow L3}$ as a red arrow and $t_{L1\rightarrow L4}$ as a light blue arrow).

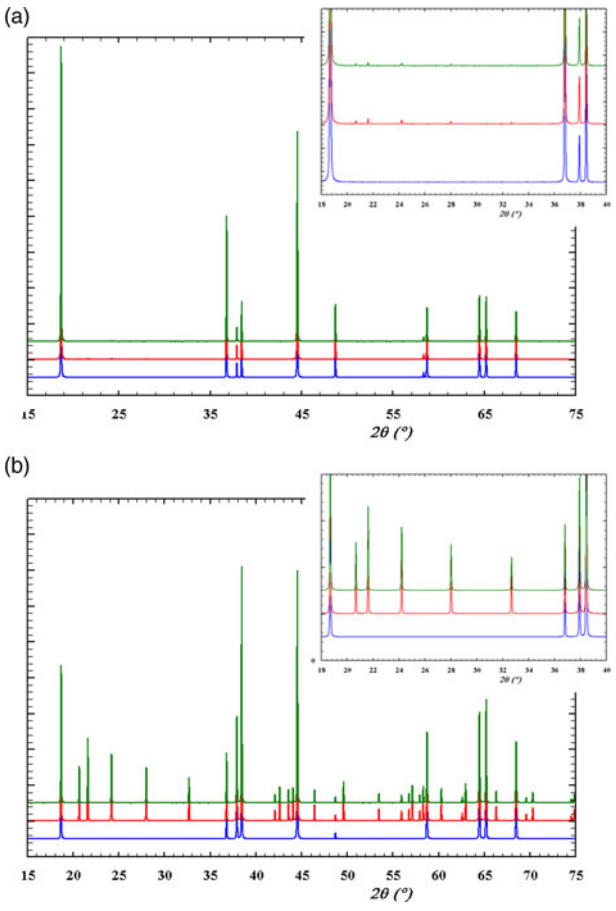

Figure 4. (Colour online) (a) XRD and (b) NPD patterns of the different models of TM cation distribution within the TM slabs: *random* (blue), *fully ordered* (red), and *honeycomb* (green) models. The insets show enlargements of the 2θ range 18°–40° focused on the superstructure reflections.

1991b), which calculates from a recursive algorithm the incoherent sum of the diffracted intensities of structures containing planar defects. In addition, FAULTS includes several modules of the Crystallographic Fortran 90 modules library (CrysFML) (Rodríguez-Carvajal and Gonzalez-Platas, 2003a, 2003b), which permits the refinement of the structural model against the experimental data, with advanced treatments for isotropic and anisotropic broadenings owing to size and strain effects (taking into account the Gaussian and Lorentzian contributions as well as the size and number of layers stacked in the crystallites).

In FAULTS, as in DIFFaX, the structure of the studied phase is described in a different way from the classical structural description using crystallographic unit cells and space groups. Indeed the layered structure has to be described as a stacking of different layers/blocks, which are stacked one on top of the others thanks to the use of stacking vectors, which occur with a given probability. This way of description of the structural model enables the user to easily introduce stacking faults by defining new layers and/or new stacking vectors.

To describe the structural models of $LiNi_{1/3}Mn_{1/3}Co_{1/3}O_2$ we used a starting monoclinic cell ($a = 4.95$ Å, $b = 8.58$ Å, $c = 5.02$ Å, and $\beta = 109.23°$), which was described in FAULTS using a vertical axis $c' = 4.739\,906$ Å and a corrective/shift transition vector of (−1/3 0 1) [for further details, refer to (Casas-Cabanas *et al.*, 2016) and the FAULTS manual provided with the program (Casas-Cabanas *et al.*, 2015)]. The monoclinic cell was deduced from the parent trigonal one (*R*-3*m*, in hexagonal setting) using the relation:

$$(\vec{a}\ \vec{b}\ \vec{c})_{\text{mono.}} = (\vec{a}\ \vec{b}\ \vec{c})_{\text{trig.}} \begin{pmatrix} 1 & 3 & -1/3 \\ -1 & 3 & 1/3 \\ 0 & 0 & 1/3 \end{pmatrix}.$$

https://doi.org/10.1017/S0885715617000033 Published online by Cambridge University Press

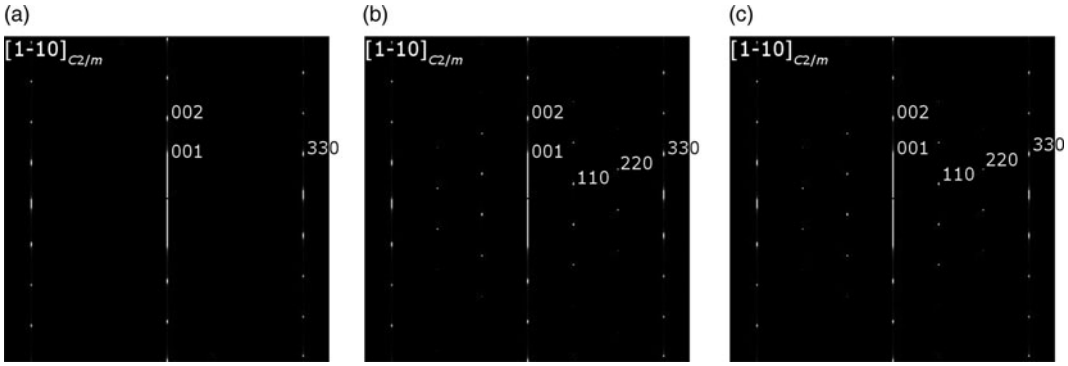

Figure 5. SADP patterns along the $[1\text{-}10]_{C2/m}$ zone axis of the different models of TM cation distribution within the TM slabs: (a) *random*, (b) *fully ordered*, and (c) *honeycomb* models.

We used two types of layers: a block of TM cations ($Ni_{1/3}Mn_{1/3}Co_{1/3}$, TM slab, layer 1) and another block containing lithium cations and oxygen anions (LiO_2, Li interslab, layer 2), as described in Table I. These layers are stacked one on top of the other by means of the transition vectors $\boldsymbol{t}_{L1\rightarrow L2} = \boldsymbol{t}_{L2\rightarrow L1} = (-1/6\ 0\ 1/2)$.

Several models of cation distributions in the TM slabs were investigated, as shown in Figure 2: (a) a *random* distribution of the TM cations over the TM sites (i.e. partial occupancy of 1/3 for each cation type for each site), which was considered as the reference model; (b) a *fully ordered* system in which each TM cation was assigned to a specific site to form a regular pavement; (c) a distribution of TM cations on α and β sites according to their cation size [Ni^{II+} on one side [ionic radius of 0.69 Å (Shannon, 1976)] and Mn^{IV+} and Co^{III+} on the other side (0.53 and 0.545 Å, respectively)] to form a *honeycomb* pattern.

Then the effect of partial cation mixing between the Li and Ni sites (0, 5, 10%) was explored for each of the three models of TM cation distribution.

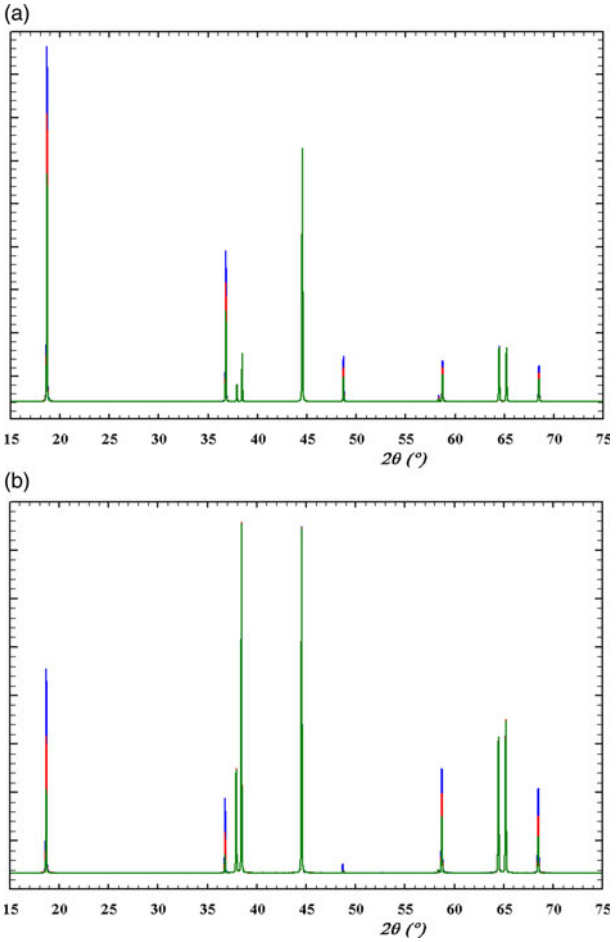

Figure 6. (Colour online) Effect of the amount of Li^{+}/Ni^{II+} cation mixing (0, 5, and 10% in blue, red, and green, respectively) on (a) the XRD and (b) the NPD patterns of the *random* model.

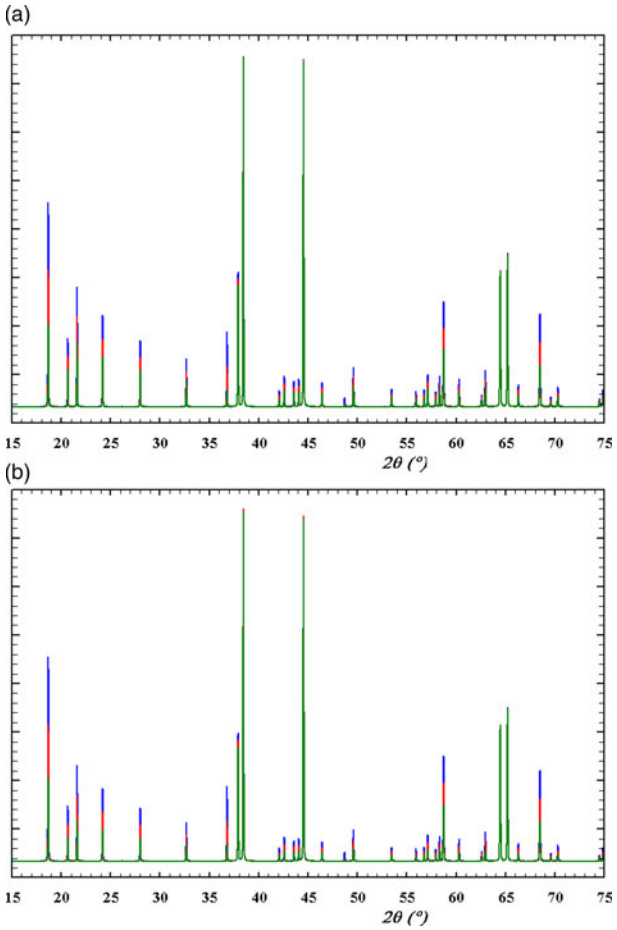

Figure 7. (Colour online) Effect of the amount of Li^{+}/Ni^{II+} cation mixing (0, 5, and 10% in blue, red, and green, respectively) on the NPD patterns of (a) the *fully ordered* and (b) the *honeycomb* models.

https://doi.org/10.1017/S0885715617000033 Published online by Cambridge University Press

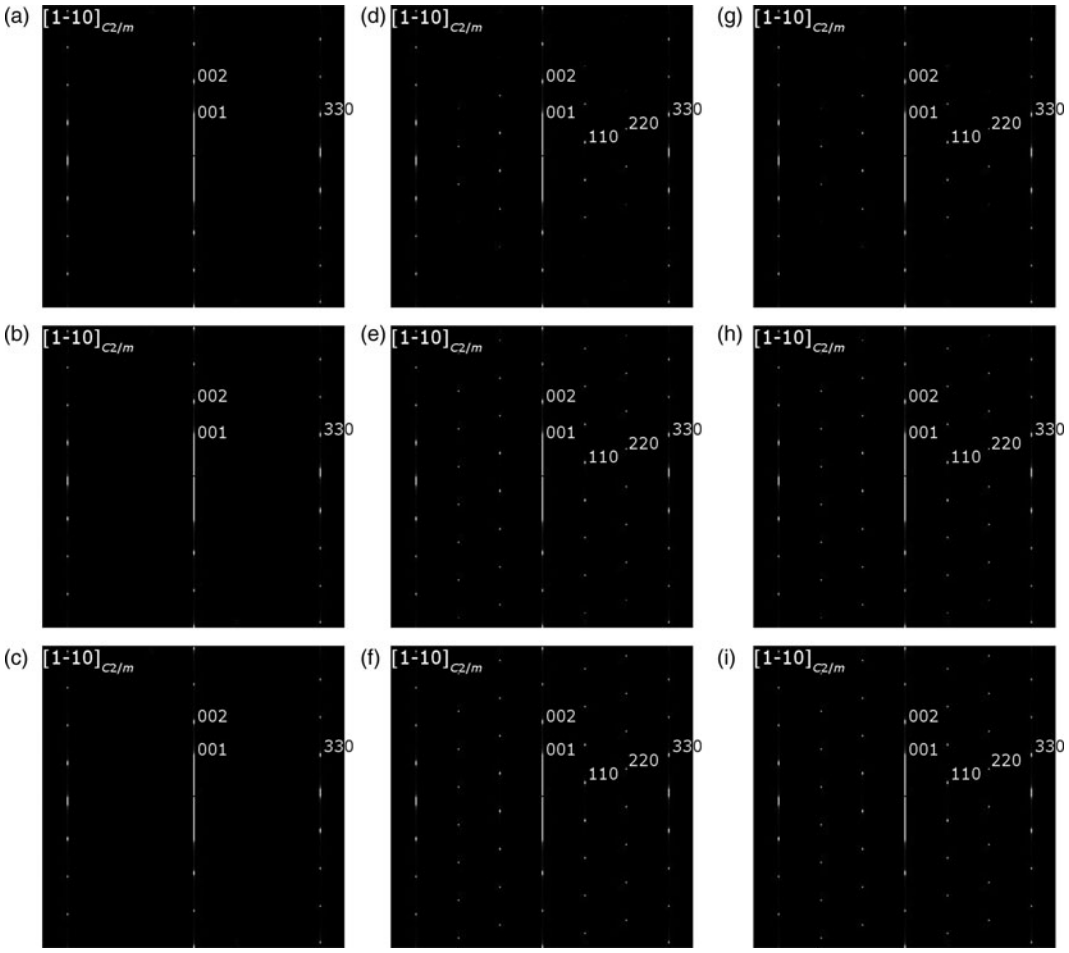

Figure 8. Effect of the amount of Li^{+}/Ni^{II+} cation mixing (a, d, and g: 0%, b, e, and h: 5% and c, f, and i: 10%) on the SADP patterns ($[1\text{-}10]_{C2/m}$ zone axis) of (a–c) the *random*, (e–g) the *fully ordered*, and (g–i) the *honeycomb* models.

Finally, the effect of stacking faults was also examined for the ordered models, with and without Li^{+}/Ni^{II+} cation mixing. For this, two additional layers (layers 3 and 4), structurally identical to layer 1, were required to describe the rotational displacements (0 1/3 0) and (0 −1/3 0) that are at the origin of the stacking faults and that were included in terms of stacking transition vectors (Figure 3 and Table I). Different values of probability of occurrence (from $p = 0$ to 33%) were given to these stacking vectors to control the amount of stacking faults occurring statistically.

Hence, combining the different TM cation distributions, the Li^{+}/Ni^{II+} cation mixing and the occurrence or absence of stacking faults, 15 different structural models were studied. FAULTS was used to simulate for each of them the XRD pattern ($\lambda_{Cu,K\alpha 1} = 1.540\,56$ Å), the NPD pattern ($\lambda = 1.54$ Å) and the selected area electron diffraction pattern (SADP, $\lambda =$ 0.0197 Å). The XRD and NPD powder patterns were generated over the 2θ range 5°–160° with a 2θ step of 0.01°. Background, number of counts and Poisson noise were generated using an offset value of 10.0 and scale factors of 1.0 and 1000.0 for XRD and NPD patterns, respectively. The SADP patterns were simulated for the $[1\text{-}10]_{C/2m}$ zone axis (i.e. plane containing the *hhl* spots), setting a maximum value of $l = 4$, the brightness to a value of 100 and the intensity data to be saved on a linear scale. These parameters were chosen so as to clearly observe the superstructure features that will be discussed further in the results sections and as a consequence a saturation line appears as an artifact at the center of the SADP patterns.

III. RESULTS AND DISCUSSION

Figure 4(a) shows the XRD pattern of a regular stacking (no stacking faults, no Li^{+}/Ni^{II+} cation mixing) of the three models of TM cation distribution within the TM slabs (layer 1). The ordering of the TM cations within the TM slabs (in both *fully ordered* and *honeycomb* models) induces the appearance of new superstructure peaks in the region 2θ 20°−35° but with a very weak intensity, which are probably hidden in the background in the case of experimental data. This loss of information about the long-range ordering in the TM slabs is due to the poor contrast between the scattering powers of the TMs. In the case of NPD patterns [Figure 4(b)], the new superstructure peaks are much more obvious over the whole 2θ range, thanks to the high contrast of scattering lengths of the TMs (Ni, 14.4 fm; Mn, −3.73 fm; Co, 2.49 fm). The intensity of the superstructure reflections is slightly lower for the *honeycomb* model with respect to the *fully ordered* model, and therefore these two models can possibly be distinguished from the refinement of experimental NPD data. In SADP patterns (Figure 5), the ordering of the TM cations within the TM slabs equally causes the appearance of

https://doi.org/10.1017/S0885715617000033 Published online by Cambridge University Press

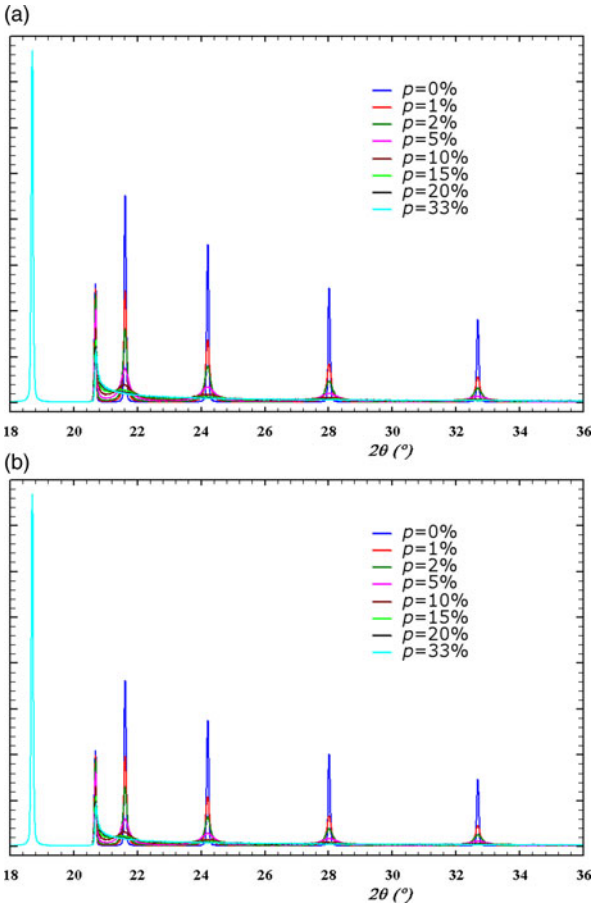

Figure 9. (Colour online) Effect of the amount of stacking faults (from $p = 0$ to 33%) on the NPD patterns of (a) the *fully ordered* model and (b) the *honeycomb* model.

additional spots along the $[001]^*_{C2/m}$ direction; however in this case the two models cannot be distinguished from the intensity of the additional spots.

Figures 6–8 show the effect of the amount of Li^+/Ni^{II+} cation mixing (0, 5, and 10%) on the XRD, NPD, and SADP patterns of the three models of TM cation distribution. As seen in Figures 6 and 7, the introduction of Li^+/Ni^{II+} cation mixing significantly weakens the intensity of the main reflections $(003)_{R\text{-}3m} \equiv (001)_{C2/m}$ at $2\theta \sim 18.7°$, $(101)_{R\text{-}3m} \equiv (130)_{C2/m}$ at $2\theta \sim 36.8°$, $(015)_{R\text{-}3m} \equiv (-132)_{C2/m}$ at $2\theta \sim 48.7°$, $(107)_{R\text{-}3m} \equiv (132)_{C2/m}$ at $2\theta \sim 58.7°$ and $(115)_{R\text{-}3m} \equiv (061)_{C2/m}$ at $2\theta \sim 68.5°$ in both XRD and NPD patterns, in agreement with the lower X-ray scattering power and neutron scattering length (−1.90 fm) of Li with respect to the TMs. The intensity changes are again more pronounced in the NPD patterns than in the XRD, and the intensity of all the superstructure reflections are also affected in the NPD patterns (Figure 7). No change is observed in the SADP patterns in the case of the *random* model [Figures 8(a)–8(c)], while an enhanced intensity of the superstructure spots is noticed with the increased amount of Li^+/Ni^{II+} cation mixing in the case of the ordered models [Figures 8(d)–8(i)].

Finally, the effect of stacking faults on the XRD, NPD, and ED patterns was examined for both of the ordered models, as shown in Figures 9 and 10. No significant change in the XRD patterns was observed (not shown here). On the contrary, the increasing amount of stacking faults induces a continuous broadening of the superstructure diffraction peaks of the NPD patterns, which eventually ends for a probability of occurrence of faulted transitions $p \geq 20\%$ in a unique asymmetric broad peak (Warren fall) typical of highly faulted structures (Figure 9). In the SADP patterns [Figures 10(a)–10(e)], the superstructure spots convert equally in diffuse scattering lines as the amount of stacking faults increases. This is in agreement with the decreasing coherent domain size of the ordered domains. Small amount of Li^+/Ni^{II+} cation mixing significantly enhanced the intensity of the diffuse scattering lines, as shown in Figure 10(f).

Our results suggest that the characterization of NMC compounds using solely X-ray diffraction can only inform

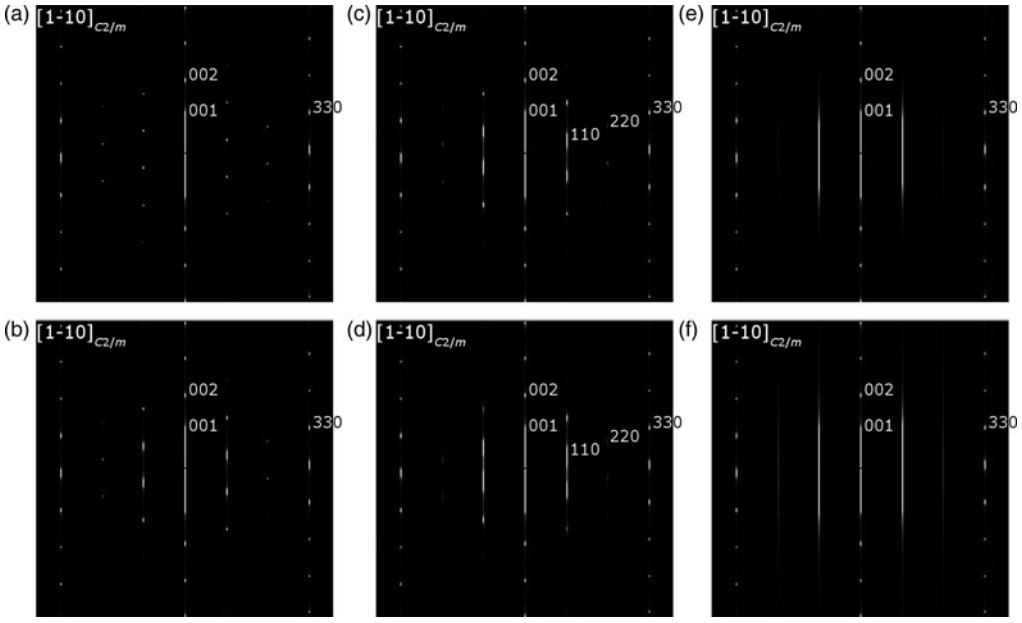

Figure 10. Effect of the amount of stacking faults (a: $p = 0\%$, b: $p = 2\%$, c: $p = 5\%$, d: $p = 10\%$, e and f: $p = 33\%$) on the SADP patterns of the *fully ordered* model, (a–e) without Li^+/Ni^{II+} cation mixing and (f) with 5% of Li^+/Ni^{II+} cation mixing.

https://doi.org/10.1017/S0885715617000033 Published online by Cambridge University Press

approximately on the amount of Li^{+}/Ni^{II+} cation mixing but totally fails in providing any information about the ordering within the TM slabs and about the regularity of stacking on these slabs, since these features do not involve any significant change in the XRD patterns. Therefore extreme care should be taken when interpreting XRD patterns of this kind of materials.

Thanks to higher contrast between the neutron scattering length and electron scattering power of the cations, NPD and ED can provide more relevant information. Superstructure reflections appear in both NPD and ED patterns when TM cations are ordered within the TM slabs. By enhancing the chemical contrast, the Li^{+}/Ni^{II+} cation mixing between TM slabs and Li interslabs significantly affects the intensity of the superstructure features in both NPD and ED patterns. Furthermore, the presence of stacking faults progressively broadens the superstructure features resulting in Warren falls and diffuse scattering lines in NPD and ED patterns, respectively.

IV. CONCLUSION

The XRD, NPD, and ED patterns of different structural models for $LiNi_{1/3}Mn_{1/3}Co_{1/3}O_2$ compounds, including cation ordering in the TM slabs, Li^{+}/Ni^{II+} cation mixing and stacking faults, were simulated using the FAULTS program. Our results show that while XRD runs short in giving reliable results on the fine microstructure of this kind of compounds, ED provides the proof of TM cation ordering within the TM slabs if such exists at least at local/short range (ED is a local probe), and even if there is no order or only weak ordering along the direction of the stacking. On the other hand, our results demonstrate that NPD should be more systematically used to characterize the long range order of the TM cations in these NMC compounds, which is not much found in the literature. Indeed, if such a TM cation ordering exists within the TM slabs, and even if there is no long-range order along the stacking direction, the intensity of the Warren peak at $2\theta \sim 20.7°$ should be sufficiently high to arise from the background of the NPD pattern and thus prove the long-range cationic ordering within the TM slabs. While NPD can probably be used to distinguish between the *fully ordered* and the *honeycomb* models, ED fails in doing so.

Finally, the results of this simulation study should orient further experimental characterization of NMC samples, and suggest that FAULTS could be successfully used to perform advanced refinement of their NPD patterns, instead of using conventional Rietveld methods, to extract the structural information that is contained in superstructure reflections that are susceptible to appear in the NPD patterns.

ACKNOWLEDGEMENTS AND COURTESIES

The authors acknowledge Juan Rodríguez-Carvajal (ILL, Grenoble, France) and Mohamed Ben Hassine (LRCS, UPJV, Amiens, France) for fruitful discussions about FAULTS and NMC compounds, respectively. They thank for the financial support from the Ministerio de Economia y Competitividad (MINECO) of the Spanish Government through the grant ENE2013-44330-R. M.R. also acknowledges MINECO for her post-doctoral fellowship (Juan de la Cierva-Formación 2014 reference number FJCI-2014-19990).

The XRD, NPD, and SADP simulations were performed with the version July 2016 of the FAULTS program. The structures were drawn and examined with the help of the visualization programs *FullProf Studio* (Rodríguez-Carvajal and Chapon, 2004) and VESTA (Momma and Izumi, 2011). The XRD and NPD patterns were plotted using the GUI program WinPLOTR (Rodríguez-Carvajal and Roisnel, 1998; Roisnel and Rodríquez-Carvajal, 2001) included in the *FullProf Suite* (Rodríguez-Carvajal, 1993a, 1993b). The SADP patterns were drawn with the image processing program ImageJ (Rasband, 1997; Abramoff *et al.*, 2004; Schneider *et al.*, 2012).

FAULTS DOWNLOAD

The FAULTS program (Casas-Cabanas *et al.*, 2006, 2015, 2016) can be obtained either as part of the *FullProf Suite* at http://www.ill.eu/sites/fullprof, or as a separate program by downloading the compressed file at http://www.cicenergigune.com/faults. The source code is also available in the CrysFML repository at http://forge.epn-campus.eu/projects/crysfml/repository/ (Rodríguez-Carvajal and Gonzalez-Platas, 2003a, 2003b).

Abramoff, M. D., Magalhaes, P. J., and Ram, S. J. (**2004**). "Image processing with imageJ," Biophotonics Int. **11**, 36–42.

Cahill, L. S., Yin, S.-C., Samoson, A., Heinmaa, I., Nazar, L. F., and Goward, G. R. (**2005**). "^{6}Li NMR studies of cation disorder and transition metal ordering in $Li[Ni_{1/3}Mn_{1/3}Co_{1/3}]O_2$ using ultrafast magic angle spinning," Chem. Mater. **17**, 6560–6566.

Casas-Cabanas, M., Rodríguez-Carvajal, J., and Palacín, M. R. (**2006**). "FAULTS, a new program for refinement of powder diffraction patterns from layered structures," Z. Kristallogr. Suppl. **23**, 243–248.

Casas-Cabanas, M., Reynaud, M., Rikarte-Ormazabal, J., Horbach, P., and Rodríguez-Carvajal, J. (**2015**). FAULTS. http://www.cicenergigune.com/faults and http://www.ill.eu/sites/fullprof

Casas-Cabanas, M., Reynaud, M., Rikarte-Ormazabal, J., Horbach, P., and Rodríguez-Carvajal, J. (**2016**). "FAULTS: a program for refinement of structures with extended defects," J. Appl. Crystallogr. **49**, 2259–2269.

Delmas, C., Fouassier, C., and Hagenmuller, P. (**1980**). "Structural classification and properties of the layered oxides," Physica *B+C* **99**, 81–85.

Guilmard, M., Pouillerie, C., Croguennec, L., and Delmas, C. (**2003**). "Structural and electrochemical properties of $LiNi_{0.70}Co_{0.15}Al_{0.15}O_2$," Solid State Ion. **160**, 39–50.

Hwang, B. J., Tsai, Y. W., Carlier, D., and Ceder, G. (**2003**). "A combined computational/experimental study on $LiNi_{1/3}Co_{1/3}Mn_{1/3}O_2$," Chem. Mater. **15**, 3676–3682.

Kim, J.-M. and Chung, H.-T. (**2004**). "The first cycle characteristics of Li $[Ni_{1/3}Co_{1/3}Mn_{1/3}]O_2$ charged up to 4.7 V," Electrochimica Acta. **49**, 937–944.

Koyama, Y., Tanaka, I., Adachi, H., Makimura, Y., and Ohzuku, T. (**2003**). "Crystal and electronic structures of superstructural $Li_{1-x}[Co_{1/3}Ni_{1/3}Mn_{1/3}]O_2$ ($0 \le x \le 1$)," J. Power Sources. **119–121**, 644–648.

Lu, Z., MacNeil, D. D., and Dahn, J. R. (**2001**). "Layered $Li[Ni_xCo_{1-2x}Mn_x]O_2$ cathode materials for lithium-ion batteries," Electrochem. Solid-State Lett. **4**, A200–A203.

Madhavi, S., Subba Rao, G. V., Chowdari, B. V. R., and Li, S. F. Y. (**2001**). "Effect of aluminium doping on cathodic behaviour of $LiNi_{0.7}Co_{0.3}O_2$," J. Power Sources **93**, 156–162.

Momma, K. and Izumi, F. (**2011**). "VESTA 3 for three-dimensional visualization of crystal, volumetric and morphology data," J. Appl. Crystallogr. **44**, 1272–1276.

Nagaura, T. and Tozawa, K. (**1990**). "Lithium ion rechargeable battery," Progr. Batter. Sol. Cells **9**, 209.

Ohzuku, T. and Makimura, Y. (**2001**). "Layered lithium insertion material of $LiCo_{1/3}Ni_{1/3}Mn_{1/3}O_2$ for lithium-ion batteries," Chem. Lett. **30**, 642–643.

Rasband, W. (**1997**). ImageJ, U. S. National Institutes of Health, Bethesda, Maryland, USA. https://imagej.nih.gov/ij/.

Rodríguez-Carvajal, J. (**1993a**). FullProf Suite. http://www.ill.eu/sites/fullprof.

Rodríguez-Carvajal, J. (**1993b**). "Recent advances in magnetic structure determination by neutron powder diffraction," Phys. B, Condens. Matter **192**, 55–69.

Rodríguez-Carvajal, J. and Chapon, L. (**2004**). FullProf Studio. http://www.ill.eu/sites/fullprof.

Rodríguez-Carvajal, J. and Gonzalez-Platas, J. (**2003a**). CrysFML repository, a Crystallographic Fortran 90 Modules Library. http://forge.epn-campus.eu/projects/crysfml/repository/.

Rodríguez-Carvajal, J. and Gonzalez-Platas, J. (**2003b**). "Crystallographic Fortran 90 modules library (CrysFML): a simple toolbox for crystallographic computing programs," Newsl. IUCr Comput. Comm. **1**, 50–58.

Rodríguez-Carvajal, J. and Roisnel, T. (**1998**). WinPLOTR. http://www.cdifx.univ-rennes1.fr/winplotr/winplotr.htm and http://www.ill.eu/sites/fullprof

Roisnel, T. and Rodríquez-Carvajal, J. (**2001**). "WinPLOTR: a windows tool for powder diffraction pattern analysis," Mater. Sci. Forum **378–381**, 118–123.

Rozier, P. and Tarascon, J. M. (**2015**). "Review—Li-rich layered oxide cathodes for next-generation Li-ion batteries: chances and challenges," J. Electrochem. Soc. **162**, A2490–A2499.

Schneider, C. A., Rasband, W. S., and Eliceiri, K. W. (**2012**). "NIH Image to ImageJ: 25 years of image analysis," Nat. Methods **9**, 671–675.

Shannon, R. D. (**1976**). "Revised effective ionic radii and systematic studies of interatomic distances in halides and chalcogenides," Acta Crystallogr. A. **32**, 751–767.

Shinova, E., Stoyanova, R., Zhecheva, E., Ortiz, G. F., Lavela, P., and Tirado, J. L. (**2008**). "Cationic distribution and electrochemical performance of $LiCo_{1/3}Ni_{1/3}Mn_{1/3}O_2$ electrodes for lithium-ion batteries," Solid State Ion. **179**, 2198–2208.

Tarascon, J.-M. and Armand, M. (**2001**). "Issues and challenges facing rechargeable lithium batteries," Nature **414**, 359–367.

Treacy, M. M. J., Newsam, J. M., and Deem, M. W. (**1991a**). "A general recursion method for calculating diffracted intensities from crystals containing planar faults," Proc. R. Soc. Lond. A. **433**, 499–520.

Treacy, M. M. J., Newsam, J. M., and Deem, M. W. (**1991b**). DIFFaX. http://www.public.asu.edu/~mtreacy/DIFFaX.html.

Tsai, Y. W., Hwang, B. J., Ceder, G., Sheu, H. S., Liu, D. G., and Lee, J. F. (**2005**). "In-situ X-ray absorption spectroscopic study on variation of electronic transitions and local structure of $LiNi_{1/3}Co_{1/3}Mn_{1/3}O_2$ cathode material during electrochemical cycling," Chem. Mater. **17**, 3191–3199.

Weaving, J. S., Coowar, F., Teagle, D. A., Cullen, J., Dass, V., Bindin, P., Green, R., and Macklin, W. J. (**2001**). "Development of high energy density Li-ion batteries based on $LiNi_{1-x-y}Co_xAl_yO_2$," J. Power Sources **97–98**, 733–735.

Whitfield, P. S., Davidson, I. J., Cranswick, L. M. D., Swainson, I. P., and Stephens, P. W. (**2005**). "Investigation of possible superstructure and cation disorder in the lithium battery cathode material $LiMn_{1/3}Ni_{1/3}Co_{1/3}O_2$ using neutron and anomalous dispersion powder diffraction," Solid State Ion **176**, 463–471.

Yabuuchi, N. and Ohzuku, T. (**2003**). "Novel lithium insertion material of $LiCo_{1/3}Ni_{1/3}Mn_{1/3}O_2$ for advanced lithium-ion batteries," J. Power Sources **119–121**, 171–174.

Yabuuchi, N., Koyama, Y., Nakayama, N., and Ohzuku, T. (**2005**). "Solid-state chemistry and electrochemistry of $LiCo_{1/3}Ni_{1/3}Mn_{1/3}O_2$ for advanced lithium-ion batteries. II. Preparation and characterization," J. Electrochem. Soc. **152**, A1434–A1440.

Yin, S.-C., Rho, Y.-H., Swainson, I., and Nazar, L. F. (**2006**). "X-ray/neutron diffraction and electrochemical studies of lithium De/re-intercalation in $Li_{1-x}Co_{1/3}Ni_{1/3}Mn_{1/3}O_2$ ($x = 0 \rightarrow 1$)," Chem. Mater. **18**, 1901–1910.

Zeng, D., Cabana, J., Bréger, J., Yoon, W.-S., and Grey, C. P. (**2007**). "Cation ordering in $Li[Ni_xMn_xCo_{(1-2x)}]O_2$-layered cathode materials: a nuclear magnetic resonance (NMR), pair distribution function, X-ray absorption spectroscopy, and electrochemical study," Chem. Mater. **19**, 6277–6289.

https://doi.org/10.1017/S0885715617000033 Published online by Cambridge University Press